Journal of Materials Chemistry B

Accepted Manuscript

ROYAL SOCIETY OF CHEMISTRY

www.rsc.org/materialsB

Evaluation of Osteogenesis and Angiogenesis of Icariin Loaded on Micro-nano Hybrid Structured Hydroxyapatite Granules as a Local Drug Delivery System for Feromal Defect Repair

Yuqiong Wu[1, 2], Lunguo Xia[3], Yuning Zhou[4], Wudi Ma[4], Na Zhang[5], Jiang Chang[5], Kaili Lin[5]*, Yuanjin Xu[4]*, Xinquan Jiang[1, 2]*

[1] Department of Prosthodontics, Ninth People's Hospital affiliated to Shanghai Jiao Tong University, School of Medicine, 639 Zhizaoju Road, Shanghai 200011, China.

[2] Oral Bioengineering and regenerative medicine Lab, Shanghai Research Institute of Stomatology, Ninth People's Hospital Affiliated to Shanghai Jiao Tong University, School of Medicine, Shanghai Key Laboratory of Stomatology, 639 Zhizaoju Road, Shanghai 200011, China.

[3] Center of Craniofacial Orthodontics, Department of Oral and Maxillofacial Surgery, Ninth People's Hospital Affiliated to Shanghai Jiao Tong University, School of Medicine, Shanghai 200011, China

[4] Department of Oral Surgery, Ninth People's Hospital Affiliated to Shanghai Jiao Tong University, School of Medicine, Shanghai Key Laboratory of Stomatology and Shanghai Research Institute of Stomatology, China

[5] State Key Laboratory of High Performance Ceramics and Superfine Microstructure, Shanghai Institute of Ceramics, Chinese Academy of Sciences, Shanghai 200050, China

Yuqiong Wu and Lunguo Xia have contributed equally to this work.

*Corresponding author

Kaili Lin, Tel.: +86 21-52412264 E-mail: lklsic@mail.sic.ac.cn

Yuanjin Xu, Tel.: +86 21-63135005 E-mail: xuyuanjin@hotmail.com

Xinquan Jiang, Tel.: +86 21 63135412 E-mail: xinquanj@aliyun.com

Abstract:

Icariin has been identified to promote osteogenic differentiation of bone mesenchymal stem cells (BMSCs). However, whether icariin could enhance angiogenic factor expression of BMSCs, which may be vital for bone repair need to be explored. Moreover, how to construct a delivery system of icariin and the repair capability in the bone defect is still unknown. In present study, the effects of icariin on the osteogenic differentiation and angiogenic factor expression of BMSCs were firstly evaluated. Moreover, new micro-nano hybrid structured HAp (micro-nano HAp) granules were fabricated to construct the delivery system of icariin, and the osteogenesis and angiogenesis of icariin loaded on micro-nano HAp granules in rat femoral plug defect model was evaluated by micro-CT measurement, sequential fluorescent labeling and histeological assay. The *in vitro* results showed that icariin significantly improved osteogenic differentiation of rat BMSCs was demonstrated by the enhanced alkaline phosphatase (ALP) activity and gene expression of runt-related transcription factor-2 (Runx2), ALP, collagen type I (Col I), osteocalcin (OCN) and OCN protein secretion. Moreover, icariin induced the angiogenic genes expression of BMSCs, such as vascular endothelial growth factor (VEGF) and angiotensin 1 (ANG1). Furthermore, the activation in AKT signaling pathways was observed in BMSCs by the treatment of icariin, and these enhancement effects could be blocked by LY294002, which suggested that AKT signaling pathway was involved in the osteogenic differentiation and angiogenic factor expression of BMSCs induced by icariin. More importantly, micro-nano HAp granules with rod-like shape were successfully fabricated and acted as delivery carrier for icariin. Consequently, icariin loaded on micro-nano HAp granules could promote new bone formation and blood vessel formation. These results demonstrated that icariin could enhance osteogenic differentiation and angiogenic factor expression of BMSCs via AKT signaling pathway, moreover, the novel micro-nano HAp granules could act as carrier for icariin to repair bone defect via enhancing osteogenesis and angiogenesis.

Key words: Icariin, micro-nano HAp granules, Bone mesenchymal stem cells, Osteogenesis, Angiogenesis, AKT signaling pathway

Introduction

Bone defects caused by tumor, traumatic injuries, and congenital defect, which adversely affect people's life, have been constantly increasing in recent years. Since growth factors play an important role in the process of bone formation, some scaffolds have been developed as delivery carriers for growth factors, and showed great bone repair ability [1,2]. However, in consideration of the expensive cost of productive and limited active period, the clinical application of exogenous growth factors is under restriction. In recent years, traditional Chinese medicine of low production cost, an empirical system of multicomponent therapeutics [3], potentially meets the demands of bone defects repair, and remedies the shortcomings of exogenous growth factors. Icariin ($C_{33}H_{40}O_{15}$, molecular weight: 676.67), the major and indicative flavonoid glucoside isolated from the herb *Epimedium pubescens*, has been identified to exert beneficial effects in promoting the osteogenesis of bone mesenchymal stromal cells (BMSCs) [4,5]. It is well known that angiogenesis is a prerequisite step to achieve the successes of bone regeneration, especially in large bone defects [6]. Recent study has demonstrated that icariin could stimulate angiogenesis of human endothelial cells [7]. However, there were no studies focusing on angiogenic factor expression of BMSCs induced by icariin. Therefore, there was a great interest in studying the osteogenesis and angiogenesis efficiency of icariin, which might greatly improve bone repair effect *in vivo*.

Previous study has showed that icariin might promote bone formation and reduce bone desorption *in vivo* by the application of a single component of icariin to a rat hypoandrogenism model [8]. Moreover, the oral administration of icariin during distraction osteogenesis could also promote new bone formation [9]. However, since the half-life of drugs and the way of blood circulation reaching to local tissue in systemic drug delivery, icariin could not maintain an appropriate concentration in the bone defect continuously. Therefore, a local sustained release system of icariin in bone defect area needs to be developed.

As a natural component of bone tissue, hydroxyapatite ($Ca_{10}(PO4)_6(OH)_2$, HAp)

biocaremic is known to be biocompatible and bioactive in living organisms, without antigenicity and cytotoxicity [10,11]. Therefore, porous scaffold and granules of HAp bioceramics have been developed and widely used in clinical bone regenerations. However, HAp is considered to be weak in osteoinductive ability, which may impact the repair capacity for bone defects[12]. Recent studies have demonstrated that due to the excellent specific surface area, micro-nano hybrid structured HAp (micro-nano HAp) granules could be applied as the carrier of drug delivery system to enhance osteoinductive ability [13].

In the present study, we hypothesized that icariin could induce osteogenic and angiogenic differentiation of BMSCs, and a new micro-nanohybrid structured HAp granules will be a suitable vehicle for constructing icariin delivery system, which could effectively promote bone formation in bone defect. In order to verify our hypothesis, the optimal concentration of icariin on the osteogenic differentiation and angiogenic factor expression of BMSCs in vitro was explored by real-time PCR and ALP activity assay as well as AKT signaling pathway, then micro-nano HAp granules with rod-like shape were fabricated to construct icariin delivery system, and filled in rat femoral defect model, osteogenesis and angiogenesis in vivo were investigated by micro-CT measurement, sequential fluorescent labeling and histological assay.

Methods and Materials

BMSCs isolation and culture

The tibia and femur were isolated from 160±10 g, male Sprague-Dawley rats (Shanghai SLAC Experimental Animal Center, China). All experimental protocols of animals in this study were approved by the Institutional Animal Care and Use Committee of the 9th People's Hospital, which is affiliated to Shanghai Jiao Tong University School of Medicine. The bone marrow was flushed out with dulbcco's modified eagle's medium (DMEM, Hyclone, USA) supplemented with 100 unit/mL penicillin, and 100 unit/mL streptomycin (Hyclone, USA). To remove the blood cells, the washouts were collected and centrifuged at 1800 rpm for 10 min. Then, the

precipitate was mixed with complete DMEM medium supplemented with 10% fetal bovine serum (FBS, Hyclone, USA), and plated into a culture flask maintained at 37 ^{o}C in 5% CO_2. Non-adherent cells were removed by changing the medium every 3 days. When large colonies formed and became confluent, the primary rat BMSCs were trypsinized with 10% trypsin-ethylene diamine tetraacetic acid (EDTA, Hyclone, USA) and passaged. BMSCs from passages 2 to 3 were used for our experiments.

Real-time PCR assay

BMSCs were plated into 12-well plates at a density of 1×10^5 cells/well and incubated for 24 h, followed by being incubated with icariin (Tauto Biotechnology Company, Shanghai, China) at concentrations of 0, 10, 20 and 40 μM, respectively. The total RNA of the cells was isolated after the treatment of icariin for 3, 7 and 10 d using the Trizol reagent (Invitrogen, USA), according to the manufacturer's recommended protocol. The RNA concentrations were determined using a NanoDrop spectrophotometer (Thermo, USA). Complimentary DNA (cDNA) was synthesized by means of a cDNA Synthesis Reverse Transcription Kit (Fermentas, Thermo, USA). Real-time PCR assay for runt-related transcription factor 2 (Runx2), alkaline phosphatase (ALP), Collagen I (Col I), osteocalcin (OCN), vascular endothelial growth factor (VEGF), Angiopoietin-1 (ANG 1) was performed using a Light-Cycler system with SYBR Premix Ex Taq^{TM} (Takara, Japan), according to the manufacturer's instructions. The conditions of the real-time PCR were as follows: denaturation at 95℃ for 10 s; 50 cycles at 95℃ for 10 s and 60℃ for 30 s; and a final dissociation stage (95℃ for 5 min) was added at the end of the amplification procedure. β-actin was used as an internal control. The data was analyzed using the comparative Ct ($2^{-\Delta\Delta Ct}$) method and expressed as a fold change respective to the control. Each sample was analyzed in triplicate. The primer sequences used in the present study are listed in Table 1.

Table.1 List of primers used and their respective forward and reverse sequences

Gene	Forward sequence Reverse sequence
β-actin	5'- GTAAAGACCTCTATGCCAACA-3' 5'- GGACTCATCGTACTCCTGCT-3'
Runx2	5'- ATCCAGCCACCTTCACTTACACC-3' 5'- GGGACCATTGGGAACTGATAGG-3'
Alkaline phosphatase (ALP)	5'- TATGTCTGGA ACCGCACTGAAC -3' 5'- CACTAGCAAGAAGAAGCCTTTGG -3'
Collagen type I(COL I)	5'- CTGCCCAGAAGAATATGTATCACC-3' 5'- GAAGCAAAGTTTCCTCCAAGACC-3'
Osteocalcin(OCN)	5'- GCCCTGACTGCATTCTGCCTCT-3' 5'- TCACCACCTTACTGCCCTCCTG-3'
Vascular endothelial growth factor (VEGF)	5'-GGCTCTGAAACCATGAACTTTCT-3' 5'-GCAATAGCTGCGCTGGTAGAC-3'
Angiopoietin-1 (ANG1)	5'-GGACAGCAGGCAAACAGAGCAGC-3' 5'-CCACAGGCATCAAACCACCAACC-3'

ALP activity assay

ALP activity quantitative and staining assay were performed at days 7 and 10 after BMSCs treated by icariin at concentrations of 0, 10, 20 and 40 μM, respectively. Samples from all groups were incubated with p-nitrophenyl phosphate (pNPP) (Beyotime, China) at 37˚C for 30 min. Absorbance values (OD) were recorded at 405 nm to detect ALP activity. Total protein contents were assessed using BCA protein assay kit (Sigma, USA), and the OD values were normalized to the bovine serum albumin (BSA, Sigma, USA) standard curve at 590 nm. ALP activity was accessed as the OD value at 405 nm per milligram of total protein. Meantime, the ALP staining

was also performed according to the manufacturer's instructions (Beyotime, China). Each sample was rinsed with PBS three times and fixed with 4% paraformaldehyde for 15 min. The sample was soaked in 0.1% naphthol AS-MX phosphate and 0.1% fast red violet LB salt in 56 mM 2-amino-2-methyl-1,3-propanediol for 30 min at 37℃, and then observed with a digital camera (ECLIPSETS 100, NIKON, Japan). All experiments were performed in triplicate.

Release kinetics of OCN from BMSCs by the treatment of icariin

BMSCs were cultured in the medium containing icariin at the concentrations of 0 and 20 μM for 3, 6, 9, 12, 15, 18 and 21 days, incubated at 37℃. At each selected time point, the supernatant was collected and stored at -80℃, then the cells were lysed on ice for 30 min in RIPA lysis buffer (Thermo, DE) supplemented with protease inhibitor cocktail, phosphatase inhibitor cocktail and phenylmethanesulfonyl fluoride (PMSF) (Kangchen, China). The protein concentration was measured using a BCA protein assay kit. The release of OCN was quantified using ELISA kits (Cusabio, China) according to the manufacturers' instructions. The volume of OCN secretion was shown as released volume/total protein of BMSCs.

Western blotting

For western blotting assay, BMSCs were cultured in the medium containing icariin at the concentrations of 20 μM for 15, 30, 60 and 120 min. The cells were lysed on ice for 30 min in RIPA lysis buffer (Thermo, DE) supplemented with protease inhibitor cocktail, phosphatase inhibitor cocktail and phenylmethanesulfonyl fluoride (PMSF) (Kangchen, China). The protein concentration was measured using a BCA protein assay kit. 20 μg of the sample was resolved on a 10% SDS-PAGE gel and electro-transferred onto polyvinylidene difluoride membrane (PVDF, Pall, USA). The membranes were blocked and incubated with appropriate primary antibodies including rabbit anti-rat AKT (CST, USA), phosphorylated-AKT (p-AKT)(Ser473) and p-AKT (Thr308)(CST, USA) at a dilution of 1:1000. For the normalization of protein loading, mouse anti-rat β-actin (Sigma, USA) antibody was used at a 1:10000

dilution. Finally, the membranes were visualized with horseradish peroxidase (HRP)-conjugated secondary antibodies (Beyotime, China, dilution, 1:1000) using the ECL plus reagents (Amersham Pharmacia Biotech, USA) by an UVItec ALLIANCE 4.7 gel imaging system.

AKT inhibitor treatment analysis

BMSCs treated with icariin at the concentration of 20 μM, were cultured in medium supplemented with AKT signaling pathway inhibitor LY294002 (CST, USA) with a final concentration of 20 μM for 7 days. Then ALP activity was measured by ALP staining and ALP activity quantitative assay as described previously. Furthermore, total RNA was isolated and synthesized cDNA, and real-time PCR was performed on Runx2, ALP, Collagen I, OCN, VEGF and ANG1 as specified previously. Meanwhile, BMSCs treated without icariin and LY294002, were identified as the control group.

Preparation of implantation constructs

The micro-nano HAp granules were fabricated by hydrothermal transformation of the α-tricalcium phosphate [α-$Ca_3(PO_4)_2$, α-TCP] granules in $CaCl_2$ aqueous solution according to our previous study [1]. The α-TCP powders were first synthesized via wet-chemical precipitation method [14]. Briefly, under vigorous stirring, the 0.5 M $Ca(NO_3)_2$•$4H_2O$ aqueous solution was added drop wise into the 0.5 M $(NH_4)_2HPO_4$ aqueous solution at the reactant molar ratio of Ca/P = 1.50. During the dropping, pH of the reaction system was controlled between 7.49 and 7.53 by addition the ammonia solution. After completely addition, the obtained white suspension was further stirred for 24 h, and followed by washing with distilled water for three times. After washing, the resultant products were dried at 120 ^{o}C for 24 h and then calcined at 900 ^{o}C for 3 h. After calcining, the powders were pressed into tablets and sintered at 1500 °C for 5 h to obtain α-TCP ceramic tablets. Then the sintered α-TCP ceramic tablets were crushed and sieved by 40 meshes and 60 meshes to obtain α-TCP granules with diameter of approximately 300-450 μm for further hydrothermal

treatment.

The 2.4 g α-TCP granules were mixed with 85 mL 0.2 M $CaCl_2$ aqueous solution. The mixtures were transferred into a 100 mL poly tetrafluoroethene (PTFE) vessel, and then the vessel was sealed in a stainless steel autoclave and heated at 180 °C for 24 h. After the hydrothermal reaction, the reaction system was cooled down to room temperature naturally. The obtained micro-nano HAp granulates were filtrated and washed by distilled water and anhydrous ethanol for three times. Finally, the products were dried at 120 ^{o}C for 24 h prior to further characterization and application.

The obtained micro-nano HAp granules were characterized by X-ray diffraction (XRD: D/max 2550 V, Rigaku, Japan) with monochromated Cu-Kαradiation. The morphology of the obtained granules was observed by scanning electron microscopy (SEM: SU8220, Japan).

The release kinetics of icariin from micro-nano HAp granules

According to the studies of growth factors, the concentrations of BMP2 applied in the bone defect model was at the multiple of 10~200 folds of that in vitro[15]. In present study, the concentrations of icariin encapsulated in the HAp granules were selected at the multiple of 10 and 100 folds of the optimized concentration in vitro (200 and 2000 μM, respectively).

The obtained 0.1 g micro-nano HAp granules were immersed in 75 μL icariin at the concentrations of 200 μM or 2000 μM overnight, respectively, followed by lypophilization to evaporate the solvent DMSO (Sigma, USA). 1 mL SBF was added to each compound and incubated at 37℃. Then the supernatant was collected and stored at 4℃ At each selected time point (1, 3, 6, 12, 24 hours, 3, 7, 14, 21, 28 days). Thereafter, the compound was resuspended in fresh SBF and incubated until the next time point. The release of icariin was quantified using HPLC system (Shimadzu 2010C, USA), and the data was presented in terms of cumulative release as a function of release time:

Cumulative amount of release (%) = $100 \times Mt/M\infty$

Where Mt was the amount of icariin released from a sample at time t. The total

amount of icariin in a sample was calculated and regarded as $M\infty$ in this study. Three samples were tested for each group and the results were reported as average values.

Rat femoral plug defect model

All surgical procedures were reviewed and approved by the Institutional Animal Care and Use Committee of the 9th People's Hospital. Nine female Sprague-Dawley rats aged 12 weeks (250±20g) were obtained from the Ninth People's Hospital Animal Center (Shanghai, China). The animals were anaesthetized by intraperitoneal injection of pentobarbital (Nembutal 4 mg/100 g), then a linear skin incision of approximately 10 mm in the distal femoral epiphysis was made bilaterally and blunt dissection of the muscles was performed to expose the femoral condyle. Then, a 3.5 mm diameter latero-lateral channel was created perpendicular to the shaft axis to destroy cancellous trabecular bone, by using a trephine bur at a slow speed irrigated under saline solution to avoid thermal necrosis. The drilled holes were rinsed by injection with saline solution in order to remove bone fragments from the cavity. Finally, a monocortical plug bone defect (3.5 mm diameter ×4 mm deep) was created in the distal region of the femur diaphysis [16]. Micro-nano HAp granules loaded with or without icariin was then gently placed to fill the drilled defects according to group allocation. Subsequently, the incision was closed as mentioned above. Thereafter, the rats were divided into three groups including micro-nano HAp granules without icariin (Group A, micro-nano HAp, n=6), micro-nano HAp granules loaded with icariin at the concentration of 200 μM (Group B, micro-nano HAp/IC-200, n=6), micro-nano HAp granules loaded with icariin at the concentration of 2000 μM (Group C, micro-nano HAp/IC-2 000, n=6).

Sequential fluorescent labeling

As for the rats of 8 weeks' observation, a polychrome sequential fluorescent

labeling for new bone formation and mineralization was performed according to our previous study[1]. Briefly, the animals were intraperitoneally injected with 25 mg/kg tetracycline hydrochloride (TE, Sigma, USA), 30 mg/kg alizarin red (AL, Sigma, USA), and 20 mg/kg calcium (CA, Sigma, USA), at 2, 4, and 6 weeks after the operation, respectively.

Microfil perfusion

To evaluate blood vessel formation, the rats of week 8 after surgery were perfused with Microfil (Flowtech, USA) after euthanasia. A long incision was made from the xyphoid down to the abdomen, and then, the abdominal aorta was exfoliated and incised, 10 mL of heparinized saline was perfused. Subsequently, 10 mL of Microfil was perfused with a rate of 2 mL/min following perfusion with saline [17].

Micro-computerized tomography (Micro-CT) measurement

Eight weeks after femur surgery, rats in each group were all sacrificed by an intraperitoneal overdose injection of pentobarbital. The specimens were fixed in formaldehyde solution. Then, the samples of each group (n=3 for each group) were examined by micro-computed tomography (micro-CT) system (μCT-80, Scanco Medical AG, Switzerland). The microfocus of the X-ray source of the μCT system had spot size 7 μm and maximum voltage 36 kV. The specimens were placed in a sample holder filled with water. They were oriented in a way that the plan of the bone was parallel to the axis of the sample holder. A high-resolution protocol (pixel matrix, 1024×1024; voxel size, 18 μm; slice thickness, 18 μm) was applied. To determine the amount of newly formed bone tissue, the best threshold for the micro-nano HAp granules alone was visually selected, followed by the determination of threshold for micro-nano HAp granules and newly formed bone together. In addition, the ranges and means of the gray level characteristic of the micro-nano HAp granules and newly formed bone were determined. The micro-nano HAp granules showed a mean gray level of 150 ± 20, whereas that of the newly formed bone was 55 ± 15. The visually determined threshold to separate micro-nano HAp granules from newly formed bone

was set at 100, thus allowing reliable distinction between the two tissue types. The amount of new bone formation was calculated by dividing newly formed bone voxels by total voxels of the initially implanted micro-nano HAp granules volume. Moreover, three-dimensional images were reconstructed, percent object volume (BV/TV), the trabecular density (Tb.N) and bone mineral density (BMD) in the bone defect were calculated by using its auxiliary histomorphometric software (Scanco Medical AG, Switzerland) [18].

In vitro observation of gross specimen blood vessels

In order to detect blood vessel formation, the samples were processed using an alcohol-methyl salicylate clearing sequence. Briefly, samples were decalcified by 10% ethylene diamine tetraacetic acid. Then digital pictures were acquired by micro-CT (μCT-80, Scanco Medical AG, Switzerland). The areas of newly formed blood vessels in the bone defect areas were measured using Image-Pro software (Plus 6.0, Media Cybernetic, USA).

Histological and histomorphometric observation

The samples of femur were dehydrated in ascending concentration of alcohols from 70% to 100%, and then embedded in polymethylmethacrylate (PMMA). Three longitudinal sections for each specimen were prepared as described in our previous study [17]. Firstly, the samples were observed for fluorescent labeling using CLSM (Leica TCS, Germany), and the fluorochrome staining for new bone formation and mineralization was quantified. The data on yellow (TE), red (AL), and green (CA) represent the bone regeneration and mineralization at weeks 2, 4, and 6 after operation, respectively. Finally, the samples were stained with Van Gieson's picro fuchsin for histological observation. The area of newly formed bone was quantified from the serial section collected from each sample, using a personal computer-based image analysis system (Image Pro Plus 6.0, Media Cybernetic, USA) and reported as a percentage of the whole bone defect area, respectively.

Statistical analysis

All experiments were performed at a minimum of three times. All measurements are expressed as mean ± SD. Significant differences between groups were determined using ANOVA and SNK post hoc or Kruskal-Wallis nonparametric procedure followed by Mann-Whitney U test for multiple comparisons based on the normal distribution and equal variance assumption test (SPSS, v.17.5, USA), while $p<0.05$ denotes statistical significance.

Result

Icariin enhanced osteogenic differentiation and angiogenic factor expression of BMSCs

In the present study, the mRNA expression of Runx2, ALP, Col I and OCN in BMSCs was detected to be improved by icariin at the concentrations of 10, 20 and 40 μM, especially in the 20 μM group ($p<0.05$, Fig. 1A, B, C, D). As the extended time of icariin treatment, the expression of Runx2 and Col I mRNA was up-regulated by icariin mostly at the concentration of 20 μM. The expression of ALP and OCN was up-regulated from days 3 to 10 by icariin, peaked at days 7. Different from the expression of osteogenic genes, the expression of VEGF mRNA was promoted as the increasing concentration of icariin, while the expression of ANG1 mRNA was induced until days 10 after the treatment of icariin ($p<0.05$, Fig. 1E, F). Both ALP quantitative activity and ALP staining assay showed the ALP activity was promoted by icariin at the concentration of 20 μM at days 7 and 10. For 40 μM group, though ALP activity was up-regulated at days 7, it was not significantly induced at days 10 (Fig. 1G, H). Moreover, the secretion of OCN was promoted significantly by icariin at the concentration of 20 μM from days 6 to days 18 ($p<0.05$, Fig. 1I), which could reach to 64.84±0.76 pg/mg at days 6, and then fluctuated from 30 pg/mg to 50 pg/mg.

AKT signaling pathway analysis

To address the role of AKT signaling pathway in the induction of osteogenic differentiation and angiogenic factor expression by icariin, we investigated the

phosphorylation of AKT signaling under icariin-stimulated conditions. Dose-dependent studies revealed that the optimal concentration of icariin was 20 μM, and then this concentration was adopted in the following studies *in vitro*. The result of western blotting showed that AKT (Thr308 site) and AKT (Ser473 site) was phosphated significantly at the first 15 and 30 min after icariin treatment, while AKT level had no significant change (Fig. 2A, B).

To further investigate the role of AKT signaling pathway in the osteogenesis stimulated by icariin, BMSCs treated with icariin were cultured in medium supplemented with AKT signaling pathway inhibitor LY294002 for 7 and 10 days. The results of Real-time PCR showed that the enhanced mRNA expression of osteogenic genes (Runx2, ALP, Col I and OCN) and angiogenic genes (VEGF and ANG1) induced by icariin were significantly inhibited by LY294002, especially at days 10 (Fig. 2C). The ALP staining and quantitative assay also demonstrated that the higher ALP activity induced by icariin was down-regulated after the treatment of LY294002 at days 7 and 10 (Fig. 2D, E). These results strongly suggest that icariin promotes osteogenic differentiation and angiogenic factor expression of rat BMSCs at least in part via the activation of AKT signaling pathways.

Characterization of micro-nano HAp granules

As shown in Fig. 3, the micrographs with low magnification image showed that obtained micro-nano HAp granules were irregular shape (Fig. 3A). More importantly, the high magnification image revealed that the topographic surface of the granules was constructed by rod-like shape with diameters between 80 nm and 3 μm, and length up to hundreds of micrometres (Fig. 3B). The XRD results confirmed that the fabricated granules could be identified as pure HAp (JCPDS card no.74-0566) phase (Fig. 3C). It is suggested that the α-TCP precursors were completely converted to HAp after hydrothermal treatment in $CaCl_2$ aqueous solution at 180 ℃ for 24 h.

The icariin release from granules was presented as percent. Fig.3D showed that the cumulative release of icariin in two different concentrations when incubated in vitro. At the initial 1 h, there was similar release efficiency in Micro-nano HAp /

IC-200 and Micro-nano HAp / IC-2 000 group, sustained at 20 % approximately. Subsequently, icariin was released in a linear upward trend in micro-nano HAp / IC-2 000 group, while the release amount of icariin reached to 88.79 ± 2.64% at the first 3 days, then it entered into the plateau. In Micro-nano HAp / IC-2 000 group, icariin released slowly in a linear upward trend at the first 3 days, reached to 60.41 ± 0.51%, then there was trace release, and reached to 63.71 ±0.85% at days 28 finally. Based on these results, it is suggested that, micro-nano HAp as a vehicle to deliver drugs could provide sustained release kinetics.

Micro-CT measurement

The micro-CT results showed that much more new bone formation was observed in group B (micro-nano HAp/IC-200) and C (micro-nano HAp/IC-2 000) as compared with control group A (micro-nano HAp) at 8 weeks after implantation (Fig.4). More importantly, the morphometrical analysis showed that significantly greater BV/TV and Tb.N was detected in micro-nano HAp/IC-2 000 group as compared with micro-nano HAp group, while significantly greater BV/TV was detected in micro-nano HAp/IC-2 000 group as compared with micro-nano HAp/IC-200 group. BMD in micro-nano HAp/IC-200 group and micro-nano HAp/IC-2 000 group was demonstrated to be greater than that in micro-nano HAp group, though there was no significant difference between micro-nano HAp/IC-200 group and micro-nano HAp/IC-2 000 group ($p<0.05$, Fig. 4).

Microfil perfusion analysis of angiogenesis

After Microfil perfusion for the samples at week 8 after operation, it was showed that the amount of blood vessel growth in micro-nano HAp/IC-200 group and micro-nano HAp/IC-2 000 group was markedly greater than that in micro-nano HAp group (Fig. 5A, B, C). Moreover, the areas of newly formed blood vessels in micro-nano HAp/IC-200 group (3.71±0.25%) and micro-nano HAp/IC-2 000 group (4.756±0.32%) were significantly larger than that in micro-nano HAp group (0.68±0.08%) ($p<0.05$), while the most new formed blood vessels was detected in

micro-nano HAp/IC-2 000 group ($p<0.05$) (Fig. 5D).

Fluorochrome labeling histomorphometrical analysis

In the present study, the fluorescent labeling analysis was processed for the samples at 8 weeks. As shown in Fig.6, the different fluorescent labeling represented new bone formation and mineralization at weeks 2, 4, and 6 after operation, respectively. At 2 weeks, the percentage of TE labeling (yellow) in micro-nano HAp/IC-2 000 group (1.79±0.14%) was higher than that in micro-nano HAp group (0.15±0.05%) and micro-nano HAp/IC-200 group (0.39±0.20%) ($p<0.05$); while there was no significant difference between micro-nano HAp group and micro-nano HAp/IC-200 group. At 4 weeks, the higher percentage of AL labeling (red) was observed in micro-nano HAp/IC-200 group (2.28±0.24%) ($p<0.05$) and micro-nano HAp/IC-2 000 group (2.45±0.47%) as compared with micro-nano HAp group (1.25±0.19%) ($p<0.05$), while there was no significant difference between micro-nano HAp/IC-200 group and micro-nano HAp/IC-2 000 group. At 6 weeks, the percentage of CA labeling (green) in micro-nano HAp/IC-2 000 group (4.95±0.38%) was higher than that in micro-nano HAp group (1.51±0.12%) and micro-nano HAp/IC-200 group (2.61±0.01%), while the percentage of CA labeling in micro-nano HAp/IC-200 group was higher than that in micro-nano HAp group ($p<0.05$).

At 2-4 weeks postoperation, the mineral apposition rate for micro-nano HAp/IC-200 group and micro-nano HAp/IC-2 000 group was 0.64±0.16 μm/day and 0.84±0.21 μm/day, respectively, with significant differences compared with the micro-nano HAp group. Due to the TE labeling for the micro-nano HAp group not being detected, we failed to present the mineral apposition rate for this group during this time period. The mineral apposition rate for micro-nano HAp/IC-2 000 group at 4-6 weeks postoperation was 1.56±0.12 μm/day, which was significantly higher than that for micro-nano HAp/IC-200 group (1.19±0.09 μm/day) and micro-nano HAp group (0.73±0.15 μm/day) (Fig.6C)

Histological analysis of bone regeneration

Analysis of undecalcified specimens stained with Van Gieson's picro fuchsine showed that there was a little newly formed bone with commencing only from the bottom of the host bone in micro-nano HAp group (6.93±0.88%) at week 8 after operation; while much more newly formed bone was detected in micro-nano HAp/IC-200 group (10.05±0.48%) and micro-nano HAp/IC-2 000 group (15.37±0.89%), with new bone formation in the center and periphery of the bone defect ($p<0.05$) (Fig. 7). Moreover, there was also significant difference between micro-nano HAp/IC-200 group and micro-nano HAp/IC-2 000 group ($p<0.05$).

Discussion

Numbers of studies have demonstrated that the growth factors, such as bone morphogenetic proteins (BMPs), fibroblast growth factors (FGFs) and platelet derived growth factor (PDGF)[19-21], could greatly promote the regeneration of bone defects. However, since the high preserved condition and production cost of growth factors, it is difficult to further promote their clinic application. Recently, the traditional Chinese medicines, which could promote osteogenesis with a high production and low cost, have been explored extensively. Among these traditional Chinese medicines, *Epimedium,* one of the herbs, has been frequently used in the treatment of bone fracture and osteoporosis for thousands of years in China. Recently, it has been demonstrated that icariin, the main active prenylated flavonol glycoside contained in the herb, could stimulate the osteogenic differentiation of BMSCs in vitro and reduced the motility and bone resorption activity of isolated osteoclasts [5,22,23]. The appropriate medicine concentration plays an important role in the research for its effect and underlying mechanism. Our previous study has demonstrated that icariin at the concentrations from 5 to 40 μM have an excellent ability in improving osteogenic differentiation within 24 h, especially at the concentration of 20 μM [24]. To further explore the osteogensis effect of icariin in the long time, the mRNA expression of osteogenic genes at 3, 7 and 10 d and ALP activity at 7 and 10 d were examined for BMSCs after the treatment of icariin at the concentrations of 0, 10, 20 and 40 μM. In the present study, the mRNA expression of osteogenic genes was all promoted by

icariin, especially at the concentration of 20 μM. Moreover, both ALP staining and quantitative analysis demonstrated ALP activity was induced by icariin at 7 and 10 d, especially at the concentration of 20 μM (Fig. 1G, H). Together with these results and our previous study, it is suggested that the osteoinduction of icariin is in concentration-dependent manner with an optimal concentration of 20 μM. As the late marker of osteogenic differentiation related to the matrix deposition and mineralization, OCN protein could be significantly induced by icariin at the concentration of 20 μM from days 6 to 18, detected by ELISA.

New bone regeneration is facilitated by angiogenesis. Blood vessels generate a distinct metabolic and molecular microenvironment, mediating growth of bone vasculature, maintaining perivascular osteoprogenitors and coupling angiogenesis to osteogenesis[25,26]. More importantly, the expression of angiogenic factors of BMSCs, such as VEGF and ANG1 could be induced by icariin in present study. VEGF plays important roles in the mobilization and recruitment, proliferation and differentiation of endothelial progenitor cells (EPC), as well as the recruitment and survival of osteoblasts [26,27]. Conversely exogenous administration of VEGF has been reported to significantly promote angiogenesis and accelerate bone healing [27]. Moreover, VEGF has been suggested to act as a central mediator for the other secreted factors, such as BMP2 and ANG1 [28-30]. ANG1 is an endothelial growth factor that functions as a ligand for the endothelial-specific receptor tyrosine kinase, Tie2. The Tie2 and VEGF receptor (VEGFR) pathways seem to work in a complementary and coordinated fashion during vascular development, with VEGF acting during the early stages of vessel development [31,32], and ANG1 acting later to promote angiogenic remolding as well as vessel maturation and endothelial cell (EC) survival [33,34]. The ability to improve osteogenic differentiation and angiogenic genes expression of icariin makes it to be an excellent candidate of growth factors for bone regeneration. Though icariin has been demonstrated to promote bone formation by oral administration [9], it seemed this strategy might not maintain icariin with appropriate concentration in the bone defect. Thus, a delivery system should be recruited to repair the bone defect effectively.

Our previous study has shown that icariin enhanced osteogenic differentiation of BMSCs via the activation of ERK, p38 and JNK MAPK signaling pathways. However, the effect of AKT signaling pathway in the osteogenic differentiation and angiogenic factor expression of icariin is not well explored. AKT signaling pathway has been reported to play a key role in the physiology and pathophysiology of various types of cells, and exert profound effect on diverse processes including cell proliferation, migration, metabolism and differentiation [35,36]. It has been reported that AKT signaling pathway played an important role in the osteogenic differentiation of progenitor cells [37,38] and the angiogenic factor expression such as VEGF, ANG1 in osteoblastic cells [38,39]. Recently, AKT pathway was also demonstrated to be involved in the osteogenic differentiation of BMSCs stimulated by icarrin [40]. However, the role of AKT signaling pathway in icariin mediated angiogenic factor expression of BMSCs has not been reported systematically. In the present study, it was shown that AKT signaling pathway became phosphorylated in icariin-treated group at Thr308 site and Ser473 site. Moreover, after AKT signaling pathway on BMSCs of icariin-treated group was inhibited by LY294002, ALP activity and the expression of osteogenic and angiogenic genes was repressed consequently. These results indicate that AKT signaling pathway plays an important role in the icariin induced osteogenesis as well as the expression of angiogenic factors on BMSCs.

HAp is chemically similar to the inorganic component of bone matrix with advantages of biocompatibility, osteoconductive capabilities in situ [41,42]. These characters have led to extensive research efforts to apply synthetic HAp as a bone substitute in biomedical application [43-45]. However, HAp is considered to be weak in osteoinductive ability, which may impact the repair capacity for bone defects [12]. In order to overcome this disadvantage, icariin, which could promote the osteogenesis and expression of angiogenic genes of rBMSCs, was loaded to HAp to improve its osteoinductive ability. Therefore, it has great clinical value to design a HAp carrier to control icariin with longer-term slow release. Numbers of studies have demonstrated that the nanostructured on the surface of HAp could have high specific surface area, which might improve loading capacity and release control function [13].

In this study, the micro-nano HAp granules with rod-like shape were fabricated via hydrothermal transformation of the α-TCP granules in $CaCl_2$ aqueous solution, and encapsulated icariin at the concentrations of 200 and 2000 μM, which were the multiple of 10 and 100 folds of optimal concentration (20 μM) in vitro, respectively. The results showed the different release efficiency of micro-nano HAp granules when it loaded with icariin at different concentrations. It is inferred that this different release efficiency may be caused by the micro-nano characteristics of HAp granules and the different adsorption amount of icariin at different concentrations in HAp granules. Since the loaded volume in 2 000 μM group was much more than that in 200 μM group, moreover, the molecular of icariin is small, and the rod-like shape of HAp granules could reticulate into a network, icariin could penetrate into the network, which could effectively slow down the release rate, especially in 2000 μM group. Therefore, it demonstrated that micro-nano HAp granules had an excellent ability to control the delivery of icariin *in vitro*.

Furthermore, in consistent with the results *in vitro*, icariin encapsulated in the micro-nano HAp granules increased the ability of HAp mediating the new bone regeneration and vessel formation in the rat femoral defect model, especially with icariin at the concentration of 2 000 μM. Since the induction of osteogenic and angiogenic expression of icariin, the more new bone and vessel *in vivo* may be induced by the sustained release of icariin when it encapsulated in micro-nano HAp granules, while the formation of vessel may further promote the regeneration of new bone. Since the enhanced effect of icariin on osteogenesis and angiogenesis, icariin was demonstrated to achieve better effect on bone repair in the rat femoral defect model. It is suggested that icariin loaded on the micro-nano HAp granules fabricated in the present study, could be applied as a novel bone-grafting biomaterial in bone defects.

Conclusions

In the present study, it is demonstrated that icariin could promote the osteogenic differentiation and expression of angiogenic factors of BMSCs, while the

concentration of 20 μM had the strongest stimulatory effect. Furthermore, the AKT signaling pathway was involved in this process. In a rat femoral defect model, icariin loaded on the micro-nano HAp granules could enhance both osteogenesis and angiogenesis *in vivo*, especially for icariin at the concentration of 2 000 μM. Present study may provide a promising strategy that micro-nano HAp granules could act as delivery vehicle for icariin to repair bone defects.

Acknowledgments

This project was supported by National Research Program of China (973 Program, 2012CB933604), National Outstanding Youth Foundation (81225006), National Natural Science Foundation of China (81170939), the Shanghai Science and Technology Development Fund (12nm0501600), Specialized Research Fund for the Doctoral Program of Higher Education (20110073110076); Biomedical Engineering Cross Research Foundation of Shanghai Jiao Tong University School (YG2012MS29), and Shanghai Jiao Tong University Doctor Innovation Program (BXJ201226).

Reference

(1) Xia, L.; Lin, K.; Jiang, X.; Fang, B.; Xu, Y.; Liu, J.; Zeng, D.; Zhang, M.; Zhang, X.; Chang, J.; Zhang, Z.: Effect of nano-structured bioceramic surface on osteogenic differentiation of adipose derived stem cells. *Biomaterials* **2014**, *35*, 8514-27.

(2) Weir, M. D.; Xu, H. H.: Osteoblastic induction on calcium phosphate cement-chitosan constructs for bone tissue engineering. *Journal of biomedical materials research. Part A* **2010**, *94*, 223-33.

(3) Cheng, K. F.; Leung, K. S.; Leung, P. C.: Interactions between modern and Chinese medicinal drugs: a general review. *The American journal of Chinese medicine* **2003**, *31*, 163-9.

(4) Song, L.; Zhao, J.; Zhang, X.; Li, H.; Zhou, Y.: Icariin induces osteoblast proliferation, differentiation and mineralization through estrogen receptor-mediated ERK and JNK signal activation. *European journal of pharmacology* **2013**, *714*, 15-22.

(5) Chen, K. M.; Ge, B. F.; Ma, H. P.; Liu, X. Y.; Bai, M. H.; Wang, Y.: Icariin, a flavonoid from the herb Epimedium enhances the osteogenic differentiation of rat primary bone marrow stromal cells. *Die Pharmazie* **2005**, *60*, 939-42.

(6) Yu, H.; VandeVord, P. J.; Mao, L.; Matthew, H. W.; Wooley, P. H.; Yang, S. Y.: Improved tissue-engineered bone regeneration by endothelial cell mediated vascularization. *Biomaterials* **2009**, *30*, 508-17.

(7) Chung, B. H.; Kim, J. D.; Kim, C. K.; Kim, J. H.; Won, M. H.; Lee, H. S.; Dong, M. S.; Ha, K. S.; Kwon, Y. G.; Kim, Y. M.: Icariin stimulates angiogenesis by activating the MEK/ERK- and PI3K/Akt/eNOS-dependent signal pathways in human endothelial cells. *Biochemical and biophysical research communications* **2008**, *376*, 404-8.

(8) Zhang, Z. B.; Yang, Q. T.: The testosterone mimetic properties of icariin. *Asian journal of andrology* **2006**, *8*, 601-5.

(9) Wei, H.; Zili, L.; Yuanlu, C.; Biao, Y.; Cheng, L.; Xiaoxia, W.; Yang, L.; Xing, W.: Effect of icariin on bone formation during distraction osteogenesis in the rabbit mandible. *International journal of oral and maxillofacial surgery* **2011**, *40*, 413-8.

(10) Wang, C.; Duan, Y.; Markovic, B.; Barbara, J.; Howlett, C. R.; Zhang, X.; Zreiqat, H.: Phenotypic expression of bone-related genes in osteoblasts grown on calcium phosphate ceramics with different phase compositions. *Biomaterials* **2004**, *25*, 2507-14.

(11) Han, Y. J.; Loo, S. C.; Lee, J.; Ma, J.: Investigation of the bioactivity and biocompatibility of different glass interfaces with hydroxyapatite, fluorohydroxyapatite and 58S bioactive glass. *BioFactors* **2007**, *30*, 205-16.

(12) Hao, Y.; Yan, H.; Wang, X.; Zhu, B.; Ning, C.; Ge, S.: Evaluation of osteoinduction and proliferation on nano-Sr-HAP: a novel orthopedic biomaterial for bone tissue regeneration. *Journal of nanoscience and nanotechnology* **2012**, *12*, 207-12.

(13) Wang, G.; Qiu, J.; Zheng, L.; Ren, N.; Li, J.; Liu, H.; Miao, J.: Sustained delivery of BMP-2 enhanced osteoblastic differentiation of BMSCs based on surface hydroxyapatite nanostructure in chitosan-HAp scaffold. *Journal of biomaterials*

science. Polymer edition **2014**, *25*, 1813-27.

(14)Liu, X.; Lin, K.; Qian, R.; Chen, L.; Zhuo, S.; Chang, J.: Growth of highly oriented hydroxyapatite arrays tuned by quercetin. *Chemistry* **2012**, *18*, 5519-23.

(15)Inoda, H.; Yamamoto, G.; Hattori, T.: Histological investigation of osteoinductive properties of rh-BMP2 in a rat calvarial bone defect model. *Journal of cranio-maxillo-facial surgery : official publication of the European Association for Cranio-Maxillo-Facial Surgery* **2004**, *32*, 365-9.

(16)Li, B.; Yoshii, T.; Hafeman, A. E.; Nyman, J. S.; Wenke, J. C.; Guelcher, S. A.: The effects of rhBMP-2 released from biodegradable polyurethane/microsphere composite scaffolds on new bone formation in rat femora. *Biomaterials* **2009**, *30*, 6768-79.

(17)Zou, D.; Zhang, Z.; He, J.; Zhang, K.; Ye, D.; Han, W.; Zhou, J.; Wang, Y.; Li, Q.; Liu, X.; Zhang, X.; Wang, S.; Hu, J.; Zhu, C.; Zhang, W.; zhou, Y.; Fu, H.; Huang, Y.; Jiang, X.: Blood vessel formation in the tissue-engineered bone with the constitutively active form of HIF-1alpha mediated BMSCs. *Biomaterials* **2012**, *33*, 2097-108.

(18)Zhao, J.; Shen, G.; Liu, C.; Wang, S.; Zhang, W.; Zhang, X.; Zhang, X.; Ye, D.; Wei, J.; Zhang, Z.; Jiang, X.: Enhanced healing of rat calvarial defects with sulfated chitosan-coated calcium-deficient hydroxyapatite/bone morphogenetic protein 2 scaffolds. *Tissue engineering. Part A* **2012**, *18*, 185-97.

(19)Kim, J. S.; Cha, J. K.; Cho, A. R.; Kim, M. S.; Lee, J. S.; Hong, J. Y.; Choi, S. H.; Jung, U. W.: Acceleration of Bone Regeneration by BMP-2-Loaded Collagenated Biphasic Calcium Phosphate in Rabbit Sinus. *Clinical implant dentistry and related research* **2014**.

(20)Behr, B.; Leucht, P.; Longaker, M. T.; Quarto, N.: Fgf-9 is required for angiogenesis and osteogenesis in long bone repair. *Proceedings of the National Academy of Sciences of the United States of America* **2010**, *107*, 11853-8.

(21)Kim, S. E.; Yun, Y. P.; Lee, J. Y.; Shim, J. S.; Park, K.; Huh, J. B.: Co-delivery of platelet-derived growth factor (PDGF-BB) and bone morphogenic protein (BMP-2) coated onto heparinized titanium for improving osteoblast function

and osteointegration. *Journal of tissue engineering and regenerative medicine* **2013**.

(22) Huang, J.; Yuan, L.; Wang, X.; Zhang, T. L.; Wang, K.: Icaritin and its glycosides enhance osteoblastic, but suppress osteoclastic, differentiation and activity in vitro. *Life sciences* **2007**, *81*, 832-40.

(23) Fan, J. J.; Cao, L. G.; Wu, T.; Wang, D. X.; Jin, D.; Jiang, S.; Zhang, Z. Y.; Bi, L.; Pei, G. X.: The dose-effect of icariin on the proliferation and osteogenic differentiation of human bone mesenchymal stem cells. *Molecules* **2011**, *16*, 10123-33.

(24) Wu, Y.; Xia, L.; Zhou, Y.; Xu, Y.; Jiang, X.: Icariin induces osteogenic differentiation of bone mesenchymal stem cells in a MAPK-dependent manner. *Cell proliferation* **2015**, *48*, 375-84.

(25) Kusumbe, A. P.; Ramasamy, S. K.; Adams, R. H.: Coupling of angiogenesis and osteogenesis by a specific vessel subtype in bone. *Nature* **2014**, *507*, 323-8.

(26) Saran, U.; Gemini Piperni, S.; Chatterjee, S.: Role of angiogenesis in bone repair. *Archives of biochemistry and biophysics* **2014**, *561*, 109-17.

(27) Street, J.; Winter, D.; Wang, J. H.; Wakai, A.; McGuinness, A.; Redmond, H. P.: Is human fracture hematoma inherently angiogenic? *Clinical orthopaedics and related research* **2000**, 224-37.

(28) Deckers, M. M.; van Bezooijen, R. L.; van der Horst, G.; Hoogendam, J.; van Der Bent, C.; Papapoulos, S. E.; Lowik, C. W.: Bone morphogenetic proteins stimulate angiogenesis through osteoblast-derived vascular endothelial growth factor A. *Endocrinology* **2002**, *143*, 1545-53.

(29) Pupilli, C.; Lasagni, L.; Romagnani, P.; Bellini, F.; Mannelli, M.; Misciglia, N.; Mavilia, C.; Vellei, U.; Villari, D.; Serio, M.: Angiotensin II stimulates the synthesis and secretion of vascular permeability factor/vascular endothelial growth factor in human mesangial cells. *Journal of the American Society of Nephrology : JASN* **1999**, *10*, 245-55.

(30) Yoshiji, H.; Kuriyama, S.; Kawata, M.; Yoshii, J.; Ikenaka, Y.; Noguchi, R.; Nakatani, T.; Tsujinoue, H.; Fukui, H.: The angiotensin-I-converting enzyme inhibitor perindopril suppresses tumor growth and angiogenesis: possible role of the vascular

endothelial growth factor. *Clinical cancer research : an official journal of the American Association for Cancer Research* **2001**, *7*, 1073-8.

(31) Auerbach, R.; Auerbach, W.: Profound effects on vascular development caused by perturbations during organogenesis. *The American journal of pathology* **1997**, *151*, 1183-6.

(32) Merenmies, J.; Parada, L. F.; Henkemeyer, M.: Receptor tyrosine kinase signaling in vascular development. *Cell growth & differentiation : the molecular biology journal of the American Association for Cancer Research* **1997**, *8*, 3-10.

(33) Asahara, T.; Chen, D.; Takahashi, T.; Fujikawa, K.; Kearney, M.; Magner, M.; Yancopoulos, G. D.; Isner, J. M.: Tie2 receptor ligands, angiopoietin-1 and angiopoietin-2, modulate VEGF-induced postnatal neovascularization. *Circulation research* **1998**, *83*, 233-40.

(34) DeBusk, L. M.; Hallahan, D. E.; Lin, P. C.: Akt is a major angiogenic mediator downstream of the Ang1/Tie2 signaling pathway. *Experimental cell research* **2004**, *298*, 167-77.

(35) Cantley, L. C.: The phosphoinositide 3-kinase pathway. *Science* **2002**, *296*, 1655-7.

(36) Martelli, A. M.; Nyakern, M.; Tabellini, G.; Bortul, R.; Tazzari, P. L.; Evangelisti, C.; Cocco, L.: Phosphoinositide 3-kinase/Akt signaling pathway and its therapeutical implications for human acute myeloid leukemia. *Leukemia* **2006**, *20*, 911-28.

(37) Chen, L. L.; Huang, M.; Tan, J. Y.; Chen, X. T.; Lei, L. H.; Wu, Y. M.; Zhang, D. Y.: PI3K/AKT pathway involvement in the osteogenic effects of osteoclast culture supernatants on preosteoblast cells. *Tissue engineering. Part A* **2013**, *19*, 2226-32.

(38) Chen, J.; Crawford, R.; Chen, C.; Xiao, Y.: The key regulatory roles of the PI3K/Akt signaling pathway in the functionalities of mesenchymal stem cells and applications in tissue regeneration. *Tissue engineering. Part B, Reviews* **2013**, *19*, 516-28.

(39) Ayalasomayajula, S. P.; Kompella, U. B.: Induction of vascular endothelial growth factor by 4-hydroxynonenal and its prevention by glutathione precursors in

retinal pigment epithelial cells. *European journal of pharmacology* **2002**, *449*, 213-20.

(40) Zhai, Y. K.; Guo, X. Y.; Ge, B. F.; Zhen, P.; Ma, X. N.; Zhou, J.; Ma, H. P.; Xian, C. J.; Chen, K. M.: Icariin stimulates the osteogenic differentiation of rat bone marrow stromal cells via activating the PI3K-AKT-eNOS-NO-cGMP-PKG. *Bone* **2014**, *66*, 189-98.

(41) Poinern, G. E.; Brundavanam, R. K.; Mondinos, N.; Jiang, Z. T.: Synthesis and characterisation of nanohydroxyapatite using an ultrasound assisted method. *Ultrasonics sonochemistry* **2009**, *16*, 469-74.

(42) LeGeros, R. Z.: Biodegradation and bioresorption of calcium phosphate ceramics. *Clinical materials* **1993**, *14*, 65-88.

(43) Hutmacher, D. W.; Schantz, J. T.; Lam, C. X.; Tan, K. C.; Lim, T. C.: State of the art and future directions of scaffold-based bone engineering from a biomaterials perspective. *Journal of tissue engineering and regenerative medicine* **2007**, *1*, 245-60.

(44) Habraken, W. J.; Wolke, J. G.; Jansen, J. A.: Ceramic composites as matrices and scaffolds for drug delivery in tissue engineering. *Advanced drug delivery reviews* **2007**, *59*, 234-48.

(45) Rajzer, I.; Menaszek, E.; Kwiatkowski, R.; Chrzanowski, W.: Bioactive nanocomposite PLDL/nano-hydroxyapatite electrospun membranes for bone tissue engineering. *Journal of materials science. Materials in medicine* **2014**, *25*, 1239-47.

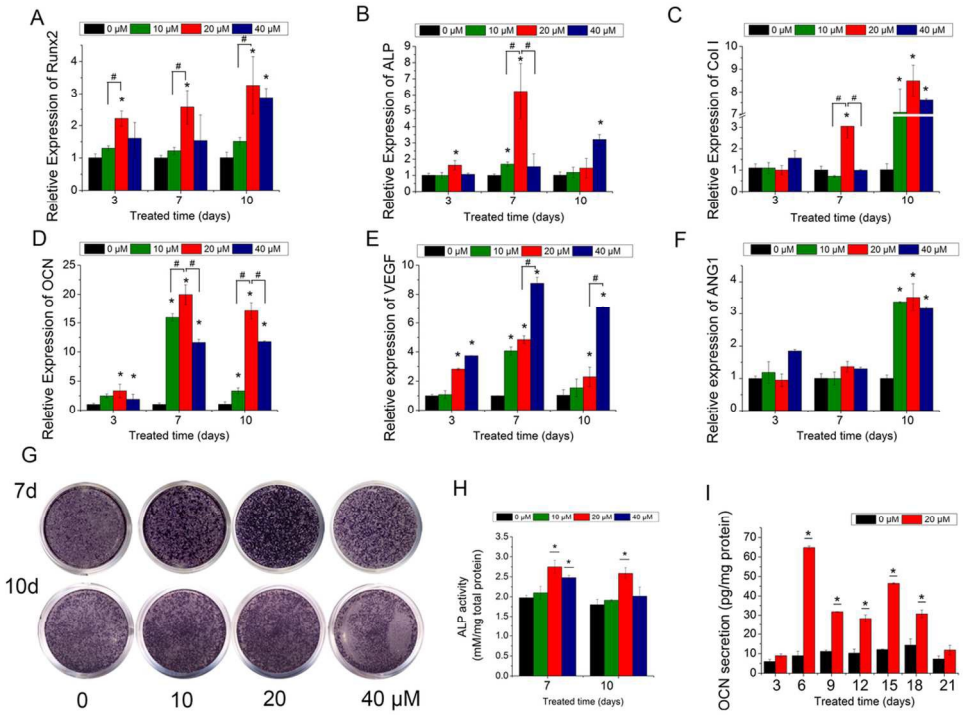

Fig. 1 Osteogenic differentiation and expression of angiogenic genes of BMSCs treated with icariin. (A-F) Rea-time PCR analysis of Runx2, ALP, collagen I, OCN VEGF and ANG1 mRNA in BMSCs treated with icariin. (G) ALP staining of BMSCs after treatment of icariin at days 7 and 10. (H) ALP activity of BMSCs treated by icariin measured by the pNPP assay at days 7 and 10. (I) OCN secretion of BMSCs treated with icariin at the concentration of 20 μM (*indicates significant differences between 0 μM and 10 ~ 40 μM groups; # indicates significant differences between 20 μM group and 10 μM or 40 μM group, $p<0.05$, n=3).
109x80mm (300 x 300 DPI)

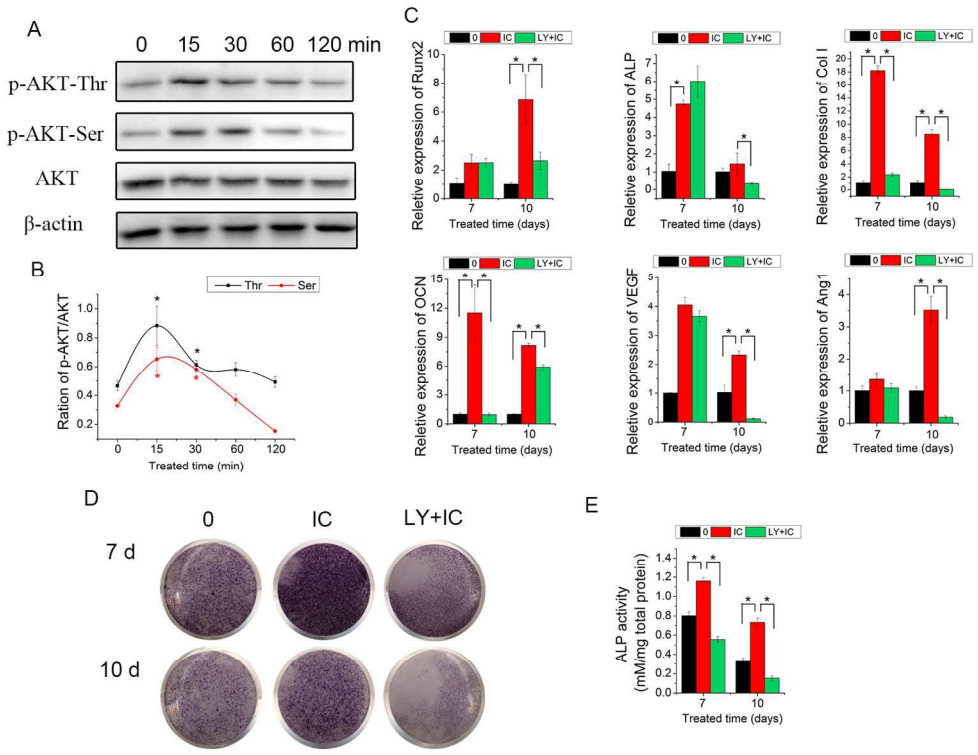

Fig. 2 Effect of AKT signaling pathway on the osteogenic differentiation and angiogenic factor expression of BMSCs treated with icariin. (A) Western blotting assay for the effect of icariin on total and phosphorylation of AKT following icariin treatment at 0, 15, 30, 60 and 120 min. (B) The ratio of p-AKT (Thr308)/AKT and p-AKT (Ser473)/AKT in Western blotting assay (* as compared the 0 min group, respectively). (C) Real-time PCR analysis of osteogenic and angiogenic genes expression of BMSCs after the treatment of icariin with or without LY294002. (D-E) ALP staining (D) and quantitative assay (E) of BMSCs after treatment of icariin with or without LY294002 (*p<0.05; * as compared the 0 μM group).
150x114mm (300 x 300 DPI)

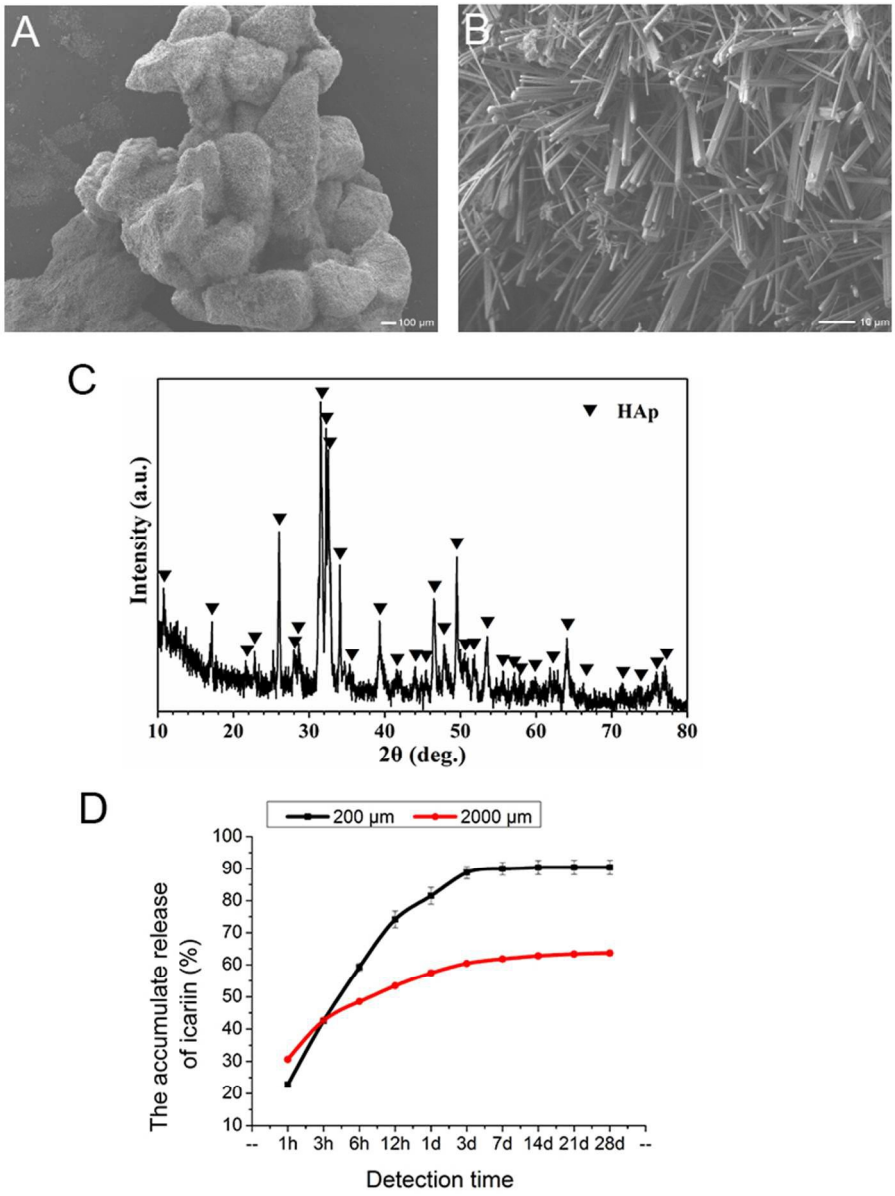

Fig. 3 Characteristics of micro-nano HAp granules. (A-B) SEM micrographs of micro-nano HAp granules (A: scale bar = 100 μm; B: topographic surfaces, scale bar =10 μm). (C) XRD patterns of micro-nano HAp granules. (D) The accumulative release percentage of icariin loaded in the micro-nano HAp granules in the concentration of 200 μM and 2000μM.
70x90mm (300 x 300 DPI)

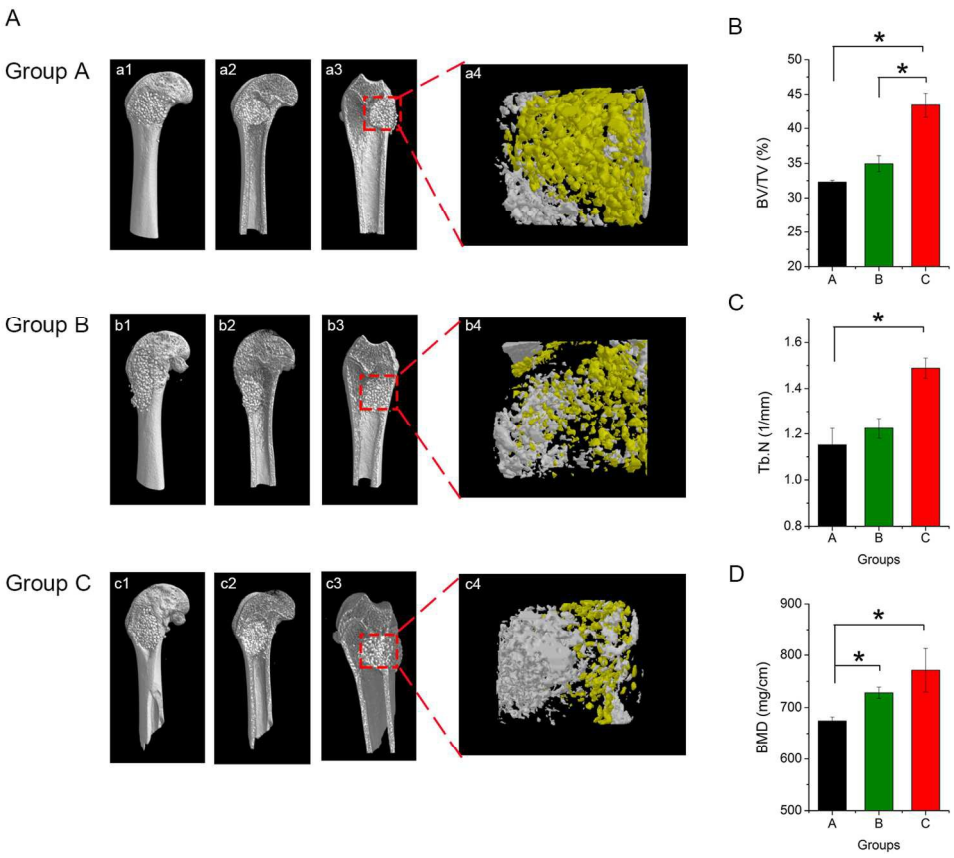

Fig. 4 Micro-CT evaluation and morphometric analysis of femoral defect repair. Representative 3D superficial (a1-c1), interior images (a2, a3, b2, b3, c2, c3) and magnified images (a4, b4, c4) of femoral defects for groups micro-nano HAp (Group A), micro-nano HAp/IC-200 (Group B) and micro-nano HAp/IC-2 000 (Group C) were taken at 8 weeks after implantation. (D-F) Percent object volume (BV/TV) (D), the trabecular density (Tb.N) (E) and bone mineral density (BMD) (F) in the bone defect by Micro-CT for each group at 8 weeks post-operation (*p<0.05).
140x119mm (300 x 300 DPI)

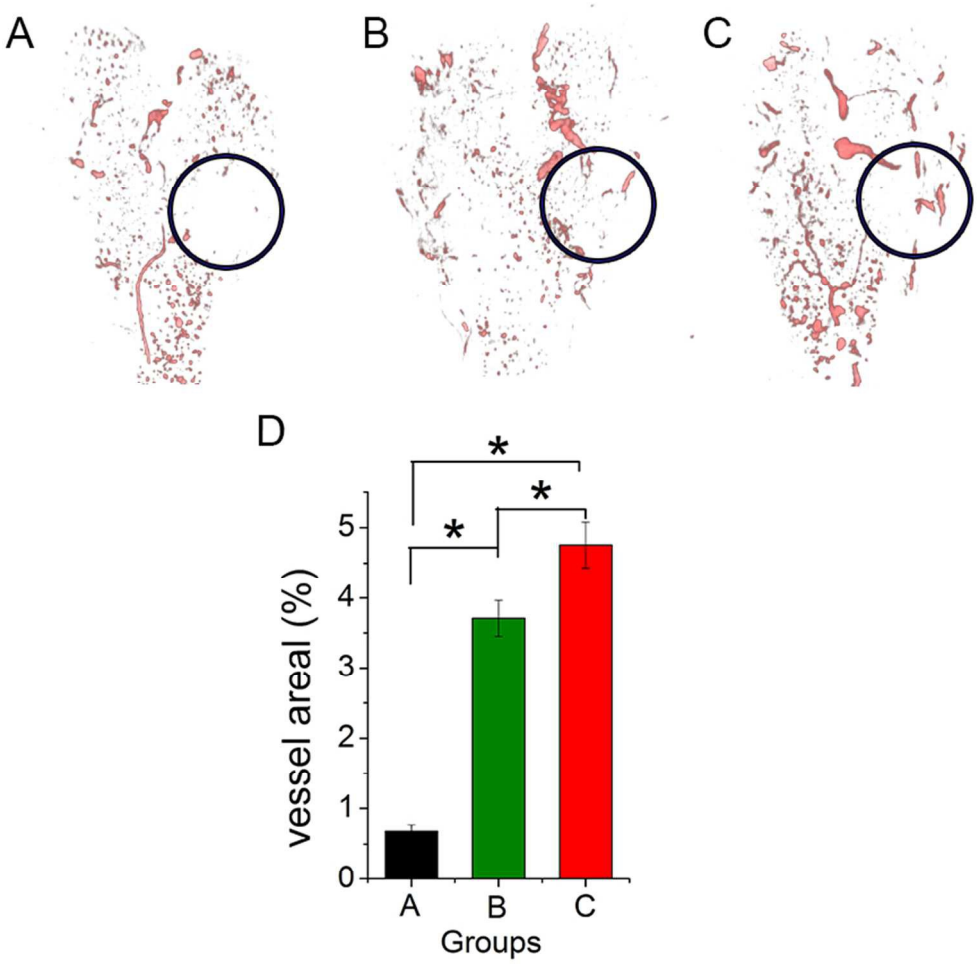

Fig.5 Histological images of newly formed blood vessels in fermoral defects for groups micro-nano HAp (A), micro-nano HAp/IC-200 (B) and micro-nano HAp/IC-2 000 (C) were taken at 8 weeks after operation. (D) Analysis of the local vessel area for different groups in the femoral defects (*p<0.05).
75x72mm (300 x 300 DPI)

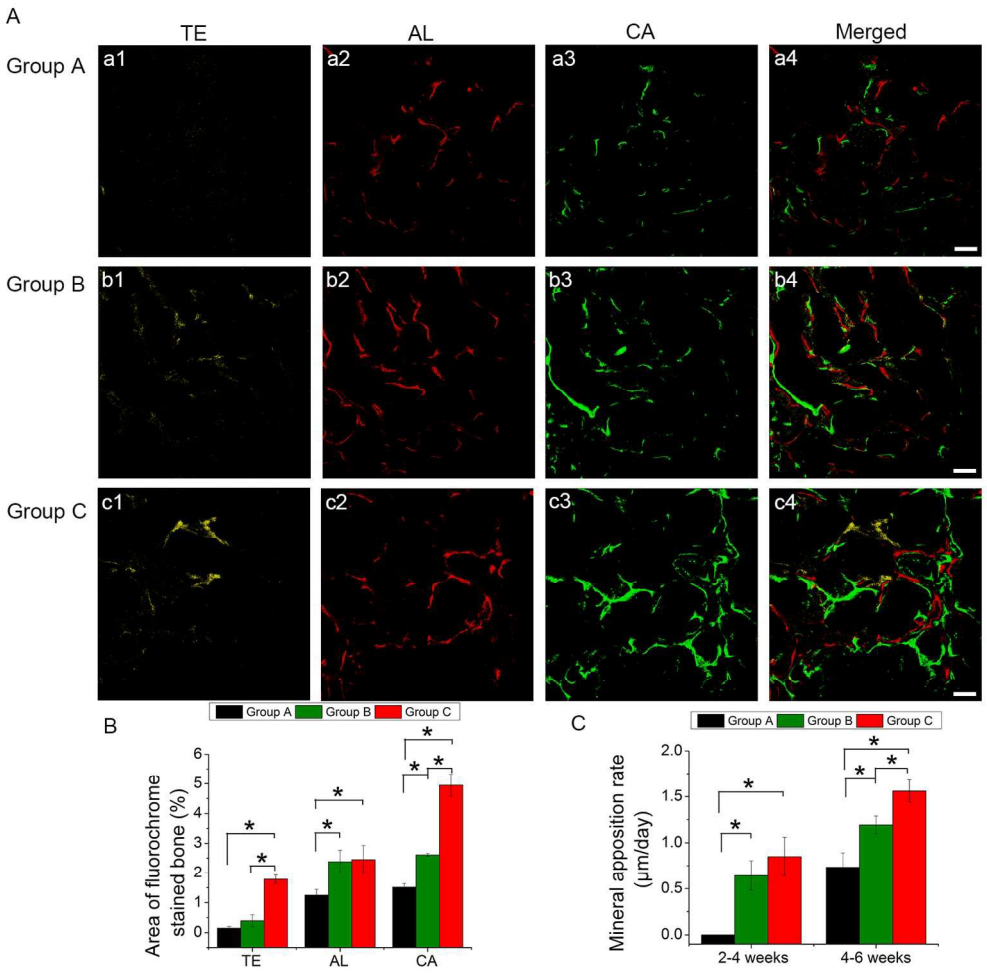

Fig. 6 Sequential fluorescent labeling of TE, AL and CA for groups Micro-nano HAp (Group A), Micro-nano HAp/IC-200 (Group B) and Micro-nano HAp/IC-2 000 (Group C) at 8 week time point. The images in yellow (TE; a1, b1, c1), red (AL; a2, b2, c2) and green (CA; a3, b3, c3) indicated the rate of bone formation and mineralization at 2, 4 and 6 weeks after operation, respectively. (a4, b4, c4) Merged images of the three fluorochromes for the same group. Scale bar = 100 μm. (B) The percentage of TE, AL and CA staining by histomorphometric analysis. (C)The mineral apposition rate for different groups in the femoral defects (*p<0.05).
150x145mm (300 x 300 DPI)

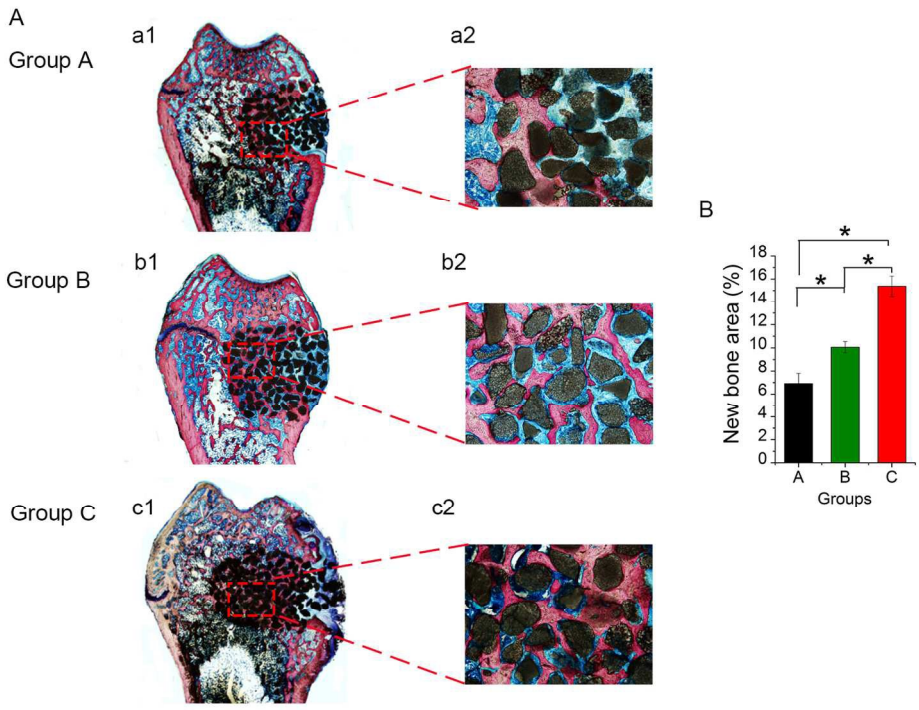

Fig. 7 Histological images of newly formed bone in femoral defects for groups Micro-nano HAp(Group A), Micro-nano HAp/IC-200 (Group B) and Micro-nano HAp/IC-2 000 (Group C) were taken at weeks 8 after operation (A, a1-c1, a2-c2); (B) The percentage of new bone area assessed at 8 weeks after implantation by histomotphometric analysis (*p<0.05; a1-c1: 40×; a2-c2: 100×)
140x99mm (300 x 300 DPI)